文章编号：1001-9014(2023)06-0711-05

DOI：10. 11972/j. issn. 1001-9014. 2023. 06. 001

High operating temperature p-on-n HgCdTe MWIR 1024×768 FPA detector

HE Tian-Ying, QIN Qiang*, KONG Jin-Cheng, QIN Gang, YANG Chao-Wei, WANG Xiang-Qian, LI Hong-Fu, WANG Qiong-Fang, LI Yong-Liang, YANG Yi-Hu, LI Yi-Min, SONG Lin-Wei, YANG Xiu-Hua, LUO Yun, CHEN Nan, HU Xu, ZHAO Jun, ZHAO Peng

(Kunming Institute of Physics, Kunming 650223, China)

Abstract: Increasing the operating temperature for infrared detectors is critical to reduce the size, weight and power of infrared (IR) systems. Such systems are essential to implement a compact and low-cost production of IR systems. For the Kunming Institute of Physics (KIP), HgCdTe standard p-on-n technology with indium doping and arsenic ion implantation technology has been optimized for many years and mid-wavelength IR (MWIR) detectors with excellent electro-optical performance were realized. This paper reports the latest results of the MWIR focal plane array (FPA) detector with a high operating temperature (HOT). Performances of the 1024×768@10 m pitch MW detector working above 150 K were presented. The detector presenting a cut-off wavelength above 4. 97 m at 150 K has been developed. The noise-equivalent temperature difference (NETD), dark current and operability at different operating temperatures were attained. Additionally, the IR image taken with the MWIR HgCdTe-based FPA and processed at an operating temperature of 150 K was presented and retained an operability of 99. 4%.

Key words: HgCdTe, HOT, MWIR, NETD, dark current

高工作温度碲镉汞 p-on-n 中波 1024×768 焦平面探测器

何天应，秦 强*，孔金丞，覃 钢，杨超伟，王向前，李红福，王琼芳，李永亮，杨翼虎，李轶民，宋林伟，杨秀华，罗 云，陈 楠，胡 旭，赵 俊，赵 鹏

(昆明物理研究所，云南 昆明 650223)

摘要：提高红外探测器的工作温度对于减小红外系统的尺寸、重量和功耗至关重要，进而实现结构紧凑和成本低廉的红外系统。昆明物理研究所多年来对掺铟和砷离子注入技术的 HgCdTe p-on-n 技术进行了优化，实现了性能优异的中波红外探测器的研制。本文报道了高工作温度中波 1024×768@10 μm 红外焦平面阵列探测器的最新结果，并介绍了在 150 K 工作温度下的器件性能。结果标明，器件在 150 K 下截止波长为 4.97 μm，并测得了不同工作温度下的 NETD、暗电流和有效像元率。此外，还展示了在 150 K 的工作温度下焦平面器件的红外图像，并呈现了 99.4% 的有效像元率。

关 键 词：碲镉汞；高工作温度；中波红外；噪声等效温差；暗电流

中图分类号：TN215　　**文献标识码**：A

Introduction

The infrared detector has been developed to the 3rd Gen sensor system using staring detector arrays operated at higher operating temperatures, with the aim of reducing size, weight and power consumption on the premise of ensuring the high performance [1-4]. With the increase of operating temperature, the reduced cooling demand of cooled infrared detector can reduce the size and power of cryocooler, economize the application cost of infrared system, and improve the environmental adaptability, reliability, and lifetime of the detector [5-9]. It has greatly optimized the IR-imaging systems which benefit the longer mission time, the easier thermal management, the re-

Received date: 2023-04-18, **revised date**: 2023-06-08　　**收稿日期**：2023-04-18，**修回日期**：2023-06-08

Foundation items: Supported by the National Key Research and Development Program of China (SQ2020YFB200190)

Biography: HE Tian-Ying (1992-), male, Nanchong, doctor. Research area involves Semiconductor infrared materials and devices. E-mail: he_tianying@qq. com

* **Corresponding author**: E-mail: 15398425155@189. cn

duced complexity of the system level and so on [10-12].

While HgCdTe offers several significant advantages, including close lattice matching for flexible control of the bandgap, readily available doping techniques, high electron mobility, high optical absorption coefficient and low carrier generation rate, making it the preferred material for demanding applications with high performance [6, 13-14]. There are mainly three kinds of device structure: Hg vacancy n-on-p structure, Au-doped n-on-n structure and extrinsic doped p-on-n structure[14, 15]. In the early stage of HOT MWIR HgCdTe products of Sofradir and AIM, the operating temperature based on Hg vacancy n-on-p structure can reach 120 K by optimizing the material quality and the fabrication process [8, 15]. The HOT MWIR HgCdTe devices based on Au-doped n-on-p structure, as the transition products for AIM, can achieve an operating temperature of 140 K limited by the Au-diffusion stability in the HgCdTe [10, 15]. The extrinsic doped p-on-n devices using arsenic ion implantation or in-situ doping have more controllable and stable impurity concentrations, which have been adopted by RVS, TIS, AIM, BAE and others to achieve a temperature around 150 K or even higher [6, 8, 11, 15-21].

In this paper, we report the study advance on the HgCdTe p-on-n MWIR FPAs. The MWIR HgCdTe FPAs showed a high operating temperature up to 150 K.

1 HgCdTe HOT MWIR FPAs

Consistent with the previous work about a 15 μm pitch 640×512 MWIR HgCdTe FPA, the detector with 1024×768 pixels and a 10 μm pixel pitch was fabricated using arsenic-ion implanted p-on-n planar junction device technology [22]. MWIR HgCdTe epitaxial layers were grown on CdZnTe (111) B substrate by liquid phase epitaxy. N-type doping was obtained by indium incorporation during growth. The n-type doping concentration was about 4×10^{14} cm^{-3}, the surface microdefect ($\Phi\geqslant5$ μm) density was less than 10 cm^{-2}, and the dislocation etch pit density was less than 5×10^{4} cm^{-2}. The epitaxial HgCdTe films have the characteristics of low dislocation density and high crystal quality, which is the basic premise of low dark current and low noise detector [23]. P-type doping was obtained by arsenic implantation and activation via a high-temperature annealing step under the condition of Hg saturation. Finally, the Hg vacancies in the materials were eliminated by low temperature Hg saturation annealing. It is noteworthy that the optimizing surface passivation and the interdiffusion annealing process are the key elements to suppress the surface-related current and noise [24]. In order to optimize the surface state of HgCdTe films, removing the dangling bonds and optimizing the annealing condition are the main method. The HgCdTe detector chip and ROIC were hybridized by a flip-chip bonding technology. Then the CdZnTe substrate was removed completely and the anti-reflection film was prepared.

To support the SWaP applications, the Dewar was designed to be compact and low in heat leakage, which was integrated to a low-power miniaturized linear Stirling cryocooler (C351). Using this feature, the optical axis is only 69.15 mm. Figure 1 shows the schematic diagram of the MWIR HgCdTe HOT integrated Dewar cooled assembly (IDCA).

Fig. 1 The photograph of the MWIR HgCdTe HOT IDCA
图1 碲镉汞中波高温组件实物图

The performance of the FPAs is determined by several key properties with an operating temperature of 150 K. The NETD is normally defined by the ratio of the temporal noise to the responsivity. The FPAs offered an NETD of ≤20 mK at 50% well fill of its 6 Me^- capacitor. The dark current was tested in a Dewar equipped with a blind cooling screen. The test results show a lower dark current of 5.2×10^{-7} A/cm^2 which is about a third of "Rule 07" [27]. This FPA has a total of 4470 defective pixels (0.6%) that were defined as defective according to criteria. The overall IDCA power consumption including all the electronics is 2.5 W at room temperature, and the cool down time is 2.5 minutes. The typical performances of the HgCdTe HOT MWIR FPA are summarized in Table 1.

2 Performance characterization

This section will present the performances of the HgCdTe HOT MWIR FPAs. If not otherwise noted, all measurements in this section are from HgCdTe 1024×768, 10 μm pitch detector arrays.

The current voltage (*IV*) plot, presented in Fig. 2, illustrates the excellent characteristics of these p-on-n photodiodes. The measurement was carried out at 150 K in front of a 293 K black body (black curve) and a 308 K black body (red curve). The *IV* curves show that the reverse breakdown voltage is higher than 1 V, demonstrating the high quality of MWIR LPE device fabrication procedure. The photodiode shows a spectral signature with a cutoff wavelength equal to 4.97 μm at 150 K (Fig. 3).

Figure 4 presents the dark-current characteristics of

Table 1　Typical performances of the HgCdTe MWIR HOT IDCA
表 1　碲镉汞中波高温组件性能参数

Parameter	Typical performance
Format & pitch	1024×768, 10 μm
FPA operating temperature	150 K
Spectral band	3.7 – 4.97 μm
Pixel capacity	4 Me^-@IWR/6 Me^-@ITR
Integration mode	ITR & IWR
Power consumption (FPAs)	173 mW
NETD	≤20 mK at 50% well fill capacity, F/2
Operability	99.4%
F#	2 or 4
Cooler	C351
Weight (IDCA)	250 g
Power consumption (IDCA)	2.5 W (at 20 ℃)
Cool down time (IDCA)	2.5 min (at 20 ℃)
Optical axis	69.15 mm

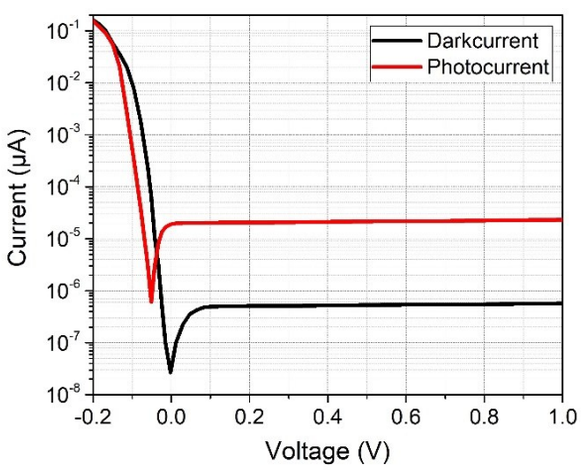

Fig. 2　Current-voltage characteristics for the MWIR HgCdTe p-on-n photodiode, 293 K black body, 150 K operating temperature
图 2　黑体温度 293 K、工作温度 150 K 时，中波碲镉汞 p-on-n 结的电流-电压特性

the p-on-n HgCdTe diodes. The dark current of the MWIR HgCdTe FPAs at different operating temperatures was tested in a Dewar equipped with a blind cooling screen, and compared with the predicted values of "Rule 07" and "Law 19" proposed by Tennant and Lee et al., with the same composition [27-28]. The dark current of the FPAs was nearly equal to the reported value of Sofradir and AIM in the range of 110-200 K. The dark current was 5.2×10^{-7} A/cm^2 at an operating temperature of 150 K, which was lower than the predicted value by "Rule 07", owing to high crystal quality HgCdTe films with low dislocation and microdefect density and low surface-related current and noise by optimizing surface passivation and interdiffusion annealing process [13, 14, 24]. The dark current at the higher temperature showed a quicker increase compared with "Rule 07" that might be due to the

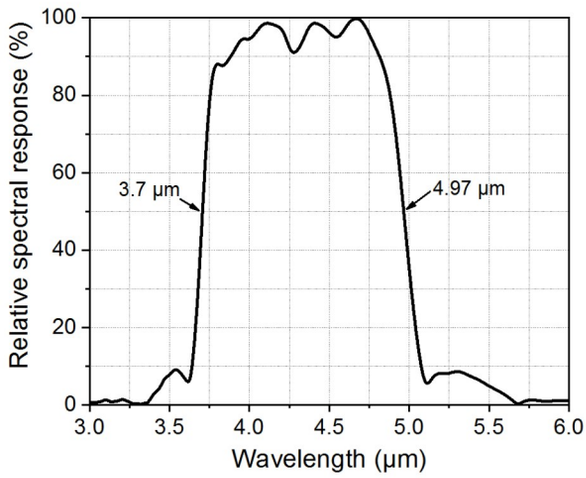

Fig. 3　The relative spectral response at 150 K operating temperature, λ_c= 4.97 μm
图 3　工作温度 150 K 时的相对光谱响应，截止波长 λ_c= 4.97 μm

increase of diffusion current and surface leakage current [7, 24-26]. The dark current at the lower temperature was inaccurate, possibly due to the reduced injection efficiency and input gate leakage in the direct injection circuit [10].

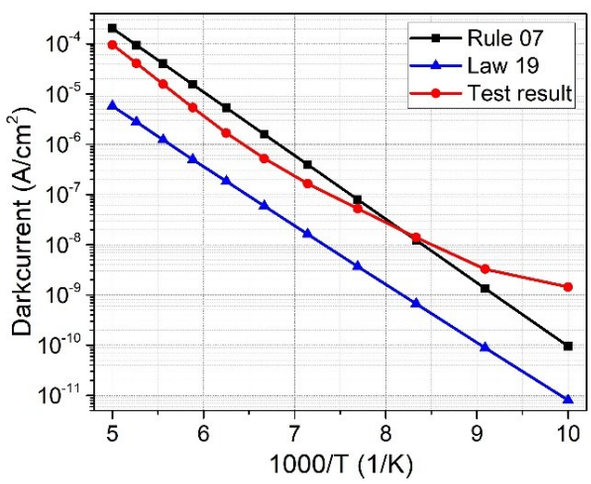

Fig. 4　The dark current dependence on the reciprocal temperature of p-on-n MWIR FPAs versus the predicted values by "Rule 07" and "Law 19"
图 4　p-on-n 结构中波焦平面器件的暗电流与工作温度关系曲线及其与"Rule 07"和"Law 19"规律对比

Meanwhile, the NETD has been measured under the half well fill condition at 308 K black body temperature for different operating temperatures in the range from 80 K to 200 K. The integration time has been adjusted for each operating temperature due to the reason that the wavelength became shorter with rising the operating temperature. Figure 5 shows the results as a function of temperature. With the operating temperature increasing, the impact on the dark current was obvious, which resulted in an NETD value slightly above 18 mK and a significant-

ly reduced integration time at 160 K. The NETD remained constant at ~17 mK up to an operating temperature of 140 K, and increased rapidly with the operating temperature exceeding 160 K. The NETD was 17.1 mK at 150 K, and the NETD histogram of the FPAs is shown in Fig. 6.

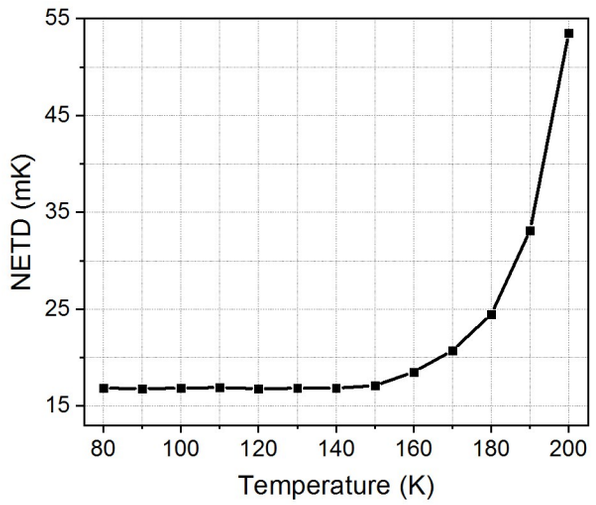

Fig. 5 The temperature dependence of the NETD for the FPAs, measured with an aperture of *F*/2 in front of a black body at a temperature of 20 ℃
图5 在*F*/2和黑体温度20 ℃条件下测得的焦平面器件NETD随工作温度变化曲线

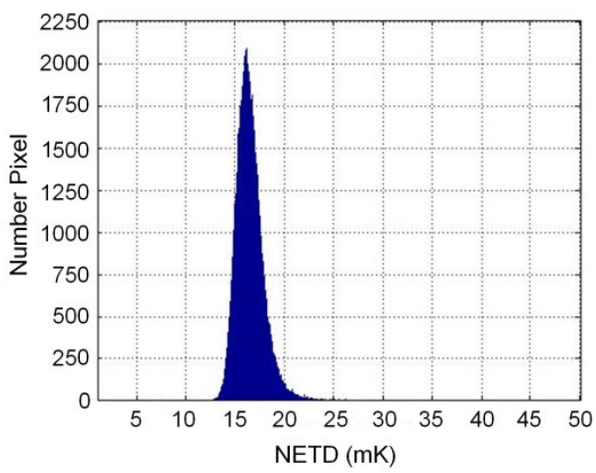

Fig. 6 The NETD histogram of FPAs at 150 K
图6 工作温度150 K时焦平面器件的NETD直方图

The operability of the FPAs, plotted in Fig. 7 as a function of the operating temperature, is better than 99.4% up to 150 K. Figure 8 shows the blind pixel distribution of FPAs at 150 K that the black dots are blind pixels.

The image at 150 K is presented in Fig. 9. It was recorded on a warm day and the image was corrected with the dead element concealment.

3 Conclusions

In conclusion, the MWIR HgCdTe HOT IDCA with

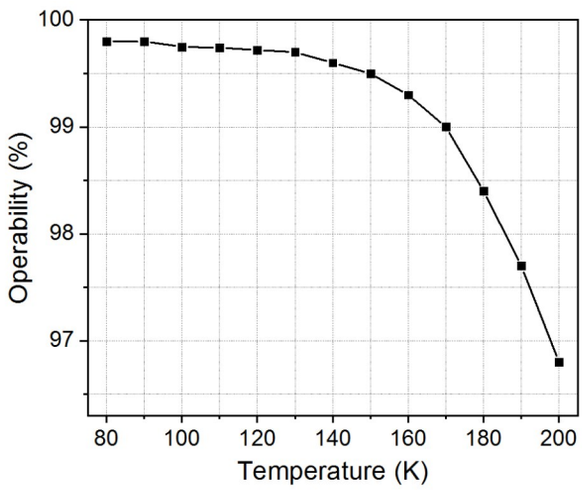

Fig. 7 The temperature dependence of the operability for FPAs
图7 焦平面器件有效像元率随工作温度变化曲线

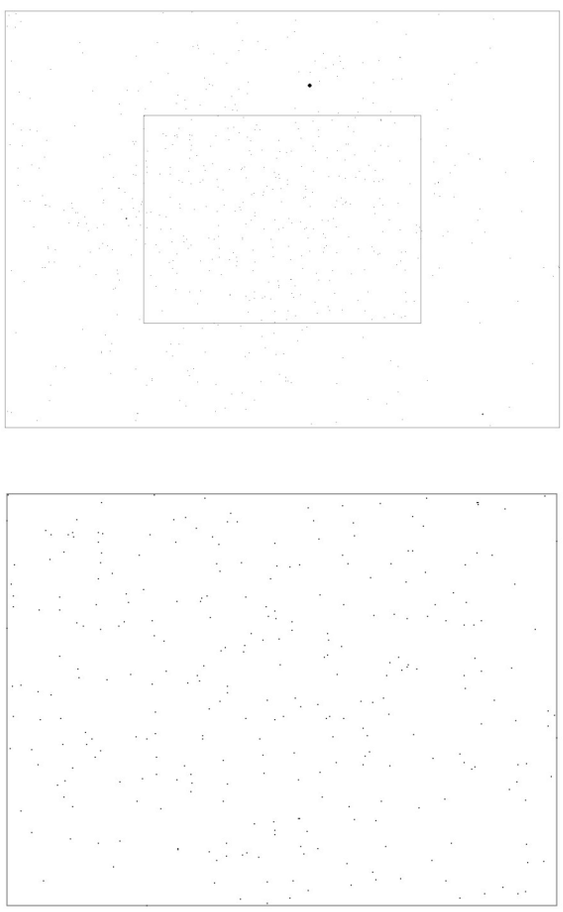

Fig. 8 The blind pixel distribution of 1 024×768 MWIR FPAs (above) and the central 512×384 area (below) at 150 K
图8 工作温度150 K时1 024×768中波焦平面器件的盲元分布(上图)及其中心512×384区域的盲元分布(下图)

1024×768 pixels and a 10 μm pixel pitch exhibits high electro-optical performance and has an operating temperature of about 150 K. The dark current is nearly equiva-

Fig. 9　The IR-image at an operating temperature of 150 K from MWIR HgCdTe HOT FPAs
图9　中波碲镉汞高温焦平面器件在150 K工作温度时的红外图像

lent to the predicted value by "Rule 07". The FPA presents a cutoff wavelength above 4.97 μm, NETD values of ~17.1 mK and operability of ~99.4% at 150 K. The optimized size, weight and power characteristics target an optical axis of 69.15 mm, a weight of 250 g and a typical power consumption of 2.5 W, which is an easy and fast integration into modern IR systems to support SWaP applications. Our next work will focus on the optimization of the device design and fabrication process to realize a higher operating temperature.

Acknowledgment

The authors wish to thank all of their colleagues at KIP who have worked together on the development of the MWIR HgCdTe HOT IDCA described in this paper. The authors would like to acknowledge internal research and development funding by KIP.

References

[1] Rogalski A, Antoszewski J, Faraone L. Third-generation infrared photodetector arrays[J]. *J. Appl. Phys.*, 2009, **105**(9): 4.
[2] Rogalsk A, Martyniuk P, Kopytko M, *et al*. Trends in performance limits of the HOT infrared photodetectors[J]. *Appl. Sci.*, 2021, **11**(2): 501.
[3] Schaake H, Kinch M, Strong R, *et al*. High operating temperature MWIR detectors[C]. Proc. of SPIE, 2010, **7608**: 907-919.
[4] Reibel Y, Taalat R, Brunner A, *et al*. Infrared SWAP detectors: pushing the limits[C]. Proc. of SPIE, 2015, **9451**: 945110.
[5] Mollard L, Destefanis G, Rothman J, *et al*. HgCdTe FPAs made by Arsenic-ion implantation[C]. Proc. of SPIE, 2008, **6940**: 69400F.
[6] James J, Haran T, Lane S. Sensor performance and cut-off wavelength tradeoffs of III-V focal plane arrays[J]. *Opto-Electron. Rev.* 2023, **31**: e144570.
[7] Lutz H, Breiter R, Figgemeier H, *et al*. Improved high operating temperature MCT MWIR modules[C]. Proc. of SPIE, 2016, **9070**: 90701D.
[8] Knowles P, Hipwood L, Pillans L, *et al*. MCT FPAs at High Operating Temperatures[C]. Proc. of SPIE, 2013, **8185**: 818505.
[9] Klipstein P, Benny Y, Cohen Y, *et al*. Type II superlattice detectors at SCD[C]. Proc. of SPIE, 2022, **11741**: 117410N.
[10] Eich D, Schirmacher W, Hanna S, *et al*. Progress of MCT detector technology at AIM towards smaller pitch and lower dark current[J]. *J. Electron. Mater.*, 2017, **46**: 5448 - 5457.
[11] Pillans L, Baker I, Kennedy R. Ultra-low power HOT MCT grown by MOVPE for handheld applications[C]. Proc. of SPIE, 2015, **9070**: 90701E.
[12] Lee D, Carmody M, Piquette E, *et al*. High-operating temperature HgCdTe: A vision for the near future[J]. *J. Electron. Mater.*, 2016, **45**(9): 4587-4595.
[13] Mollard L, Destefanis G, Bourgeois G, *et al*. Status of p-on-n arsenic-implanted HgCdTe technologies[J]. *J. Electron. Mater.*, 2011, **40**(8): 1830-1839.
[14] Kinch M. The Future of Infrared: III - Vs or HgCdTe?[J]. *J. Electron. Mater.*, 2005, **44**(9): 2969 - 2976.
[15] Lutz H, Breiter R, Eich D, *et al*. Small pixel pitch MCT IR-modules[C]. Proc. of SPIE, 2016, **9819**: 98191Y.
[16] Jeckells D, Kennedy R, Bains S, *et al*. Further developments of 8μm pitch MCT pixels at Finmeccanica (formerly Selex ES)[C]. Proc. of SPIE, 2016, **9819**: 98191X.
[17] Rubaldo L, Taalat R, Berthoz J, *et al*. Recent advances on long wave p-on-n HgCdTe infrared Technology[C]. Proc. of SPIE, 2017, **10111**: 101112H.
[18] Smith K, Wehner J, Graham R, *et al*. High operating temperature mid-wavelength infrared HgCdTe photontrapping focal plane arrays[C]. Proc. of SPIE, 2012, **8353**: 83532R.
[19] Gravrand O, Lobre C, Santailler J, *et al*. Design of a small pitch (7.5μm) MWIR MCT array operating at high temperature (130K) with high imaging performances[C]. Proc. of SPIE, 2022, **12107**: 121070U.
[20] Starr B, Mears L, Fulk C, *et al*. RVS large format arrays for astronomy[C]. Proc. of SPIE, 2016, **9915**: 929-942.
[21] Jerrama P, Beletic J. Teledyne's high performance infrared detectors for space missions[C]. Proc. of SPIE, 2019, **11180**: 1270-1279.
[22] Qin G, Qin Q, Kong J C, *et al*. High operating temperature HgCdTe mid-wavelength infrared detectors[C]. Proc. of SPIE, 2023, **12617**: 231-239.
[23] Jiao C, Zhao S, Qiang X, *et al*. The relationship of lattice mismatch the HgCdTe/CdZnTe with X-ray diffraction[J]. *Laser Infrared*, 2007, **37**: 910-914.
[24] Hu W D, Chen X, Ye Z, *et al*. A hybrid surface passivation on HgCdTe long wave infrared detector with in-situ CdTe deposition and high-density hydrogen plasma modification[J]. *Appl. Phys. Lett.*, 2011, **99**: 091101.
[25] Li Q, Xie R, Wang F, *et al*. SRH suppressed P-G-I design for very long-wavelength infrared HgCdTe photodiodes[J]. *Opt. Express*, 2022, **30**: 16509-16517.
[26] Hu W D, Ye Z, Liao L, *et al*. 128 × 128 long-wavelength/mid-wavelength two-color HgCdTe infrared focal plane array detector with ultralow spectral cross talk[J]. *Opt. Lett.*, 2014, **39**: 5184-5187.
[27] Tennant W, Lee D, Zandian M, *et al*. MBE HgCdTe technology: A very general solution to IR detection, described by ''Rule 07'', a very convenient heuristic[J]. *J. Electron. Mater.*, 2008, **37**: 1406 - 1410.
[28] Lee D, Dreiske P, Ellsworth J, *et al*. Law 19 - the ultimate photodiode performance metric[C]. Proc. of SPIE, 2020, **11407**: 93-105.